Coarsening and pattern formation during true morphological phase separation in unstable thin films under gravity

Avanish Kumar,[1] Chaitanya Narayanam,[2] Rajesh Khanna,[2,*] and Sanjay Puri[1]
[1]*School of Physical Sciences, Jawaharlal Nehru University, New Delhi 110067, India*
[2]*Department of Chemical Engineering, Indian Institute of Technology Delhi, New Delhi 110016, India*
(Received 3 August 2017; revised manuscript received 9 December 2017; published 22 December 2017)

We address in detail the problem of true morphological phase separation (MPS) in three-dimensional or $(2+1)$-dimensional unstable thin liquid films (>100 nm) under the influence of gravity. The free-energy functionals of these films are asymmetric and show two points of common tangency, which facilitates the formation of two equilibrium phases. Three distinct patterns formed by relative preponderance of these phases are clearly identified in "true MPS". Asymmetricity induces two different pathways of pattern formation, viz., defect and direct pathway for true MPS. The pattern formation and phase-ordering dynamics have been studied using statistical measures such as structure factor, correlation function, and growth laws. In the late stage of coarsening, the system reaches into a scaling regime for both pathways, and the characteristic domain size follows the Lifshitz-Slyozov growth law [$L(t) \sim t^{1/3}$]. However, for the defect pathway, there is a crossover of domain growth behavior from $L(t) \sim t^{1/4} \rightarrow t^{1/3}$ in the dynamical scaling regime. We also underline the analogies and differences behind the mechanisms of MPS and true MPS in thin liquid films and generic spinodal phase separation in binary mixtures.

DOI: 10.1103/PhysRevE.96.062804

I. INTRODUCTION

Far-from-equilibrium systems exhibit interesting spatiotemporal evolutions through formation of complex structures and patterns [1–4]. This behavior is universal and wide ranging, existing from nano- to macroscale in length and over large time scales [5,6]. These systems have great scientific and technological applications [7–9]. The properties of such systems are governed by their components as well as the kinetic processes leading to their formation. This has led to profound research interest in the kinetics of phase separation, that is, the evolution of a homogeneous mixture, from unstable or metastable state, to its segregated state [7,10–13]. These systems are initially rendered thermodynamically unstable due to sudden change in external parameters like temperature, pressure, magnetic field, etc.

Thin films constitute an important class of such systems, and phase separation in thin liquid and polymer films is an important area in the study of kinetics of phase transitions [14–22]. Domain growth kinetics in thin solid films has also been the subject of extensive research [23–25]. Thin liquid films which are initially far from equilibrium separate into a low-curvature flat-film phase and high-curvature circular droplets when subjected to random fluctuations [26,27]. This phenomenon is known as morphological phase separation (MPS) [28,29] and is observed in thin-liquid-film systems with free-energy functionals having one finite minimum, as shown in Fig. 1. For MPS in thin liquid films, the flat-film phase is the only equilibrium phase, and the nonequilibrium droplets are considered to be a *defect* rather than a *phase* [27]. The second equilibrium phase, which corresponds to the second minima in the double tangent construction, can be obtained only at infinity (Fig. 1). In the absence of a second finite minimum, the system is always in nonequilibrium state with diffused interfaces. There is an absence of well-defined domains and domain boundaries corresponding to the second phase. It was shown in earlier studies [29] that, even in the late stages of coarsening, the system does not reach the dynamical scaling regime. It was found that the scaled structure factor and the equal time correlation functions also do not exhibit dynamical scaling. Further, the growth of the average domain sizes does not follow the predicted LS growth law [$L(t) \sim t^{1/3}$] for diffusive dynamics [30].

For MPS in thin liquid films below 100 nm, the role of gravity is negligible in determining the morphological evolution. However, when slightly thicker films (>100 nm) undergo MPS, the coarsening defects can rise to submicrometer ranges, upon which the effect of gravity can no longer be neglected. The free-energy functional for these films with gravity included (Fig. 2) yields two finite heights, $P1$ and $P2$, which are obtained from Maxwell's double-tangent construction [31,32]. These correspond to the formation of two equilibrium phases with finite thicknesses during the MPS of thin liquid films, i.e., a lower-thickness phase corresponding to $P1$ and a higher-thickness phase corresponding to $P2$. This MPS of thin liquid films resulting in two finite equilibrium phases has been termed as "true MPS" [32] in order to differentiate from the case of normal MPS, where there is only one finite equilibrium phase.

In our present work, we investigate true MPS in three-dimensional or $(2+1)$-dimensional thin-liquid-film systems under the influence of gravity. We use the analogy of generic spinodal phase separation to explain the domain growth kinetics during true MPS of thin liquid films.

The organization of the paper is as follows. In Sec. II, we describe the mathematical model for the evolution of thin liquid films under gravity. In Sec. III, we present detailed descriptions of pattern formation and morphological evolutions during true MPS. We also present the growth laws of evolving patterns in terms of statistical measures such as correlation function, structure factor, and the domain size.

*rajkh@chemical.iitd.ac.in

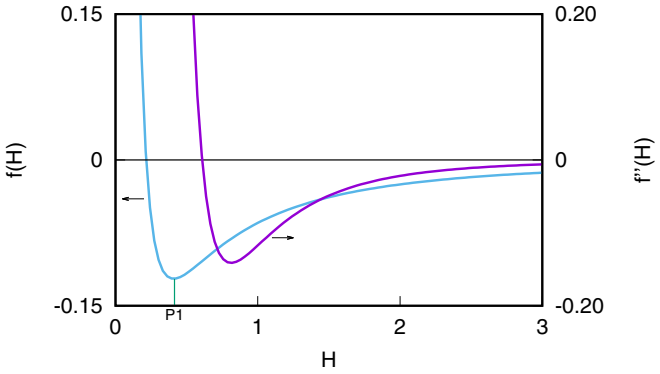

FIG. 1. Variation of dimensionless free energy $f(H)$ and its second derivative $f''(H)$ with film thickness H for a system given by Eq. (3) with $G = 0$. The parameters are $B = -0.1$ and $D = 0.5$. $P1$ represents the minimum of the free-energy functional. For $f''(H) < 0$, the homogeneous thin liquid film is unstable and spontaneously segregates into a flat film given by equilibrium thickness $P1$ and nonequilibrium circular droplets.

Finally, in Sec. IV we conclude the paper with a brief summary of our work.

II. MATHEMATICAL MODEL AND SIMULATION

The thin-film evolution equation, which is derived by the application of lubrication approximation [14] to hydrodynamic equations of motion, can be written in a dimensionless form similar to the Cahn-Hilliard equation [33,34] as

$$\frac{\partial}{\partial t}H(X,Y,t) = \vec{\nabla}\cdot\left[M\vec{\nabla}\left(\frac{\partial F}{\partial H}\right)\right], \tag{1}$$

where $H(X,Y,t)$ is the height of the film at the point (X,Y) on a $2d$ substrate and time t. The mobility in Eq. (1) is height dependent and is given by $M(H) = H^3$ corresponding to the no-slip condition of the Stokes flow. The dimensionless free-energy functional is given by

$$F(H) = \int dXdY\left[f(H) + \frac{1}{2}\left(\vec{\nabla}H\right)^2\right], \tag{2}$$

where the square gradient term represents the interfacial tension and $f(H)$ is the local free energy. At equilibrium, the free energy tends to lower to its minimum by minimizing the interfaces. The square gradient term represents the energy cost for these interfaces. It incorporates the spatial inhomogeneities or discontinuities in the system. The thin liquid film is supported on an apolar solid substrate with a nanocoating. The substrate provides long-range Lifshitz-Van der Waals attraction, and coating provides relatively shorter-range Lifshitz-Van der Waals repulsion. The corresponding free energy can be generalized to include the effect of gravity on the film thickness [32] as

$$f(H) = -\frac{1}{6}\left[\frac{1-B}{(H+D)^2} + \frac{B}{H^2} - GH^2\right]. \tag{3}$$

In Eq. (3), $D = \delta/h_0$ is the dimensionless thickness of coating, $B = A_c/A_s$ is a system-specific constant that is always negative, and $G = 2\pi\rho g h_0^4/|A_s|$ is the force corresponding to gravity. Here, δ is the coating thickness, h_0 is the thickness of the liquid film, and A_c and A_s are the Hamaker constants [35] corresponding to coating and the substrate, respectively. Further, ρ is the density of the liquid and g is the acceleration due to gravity.

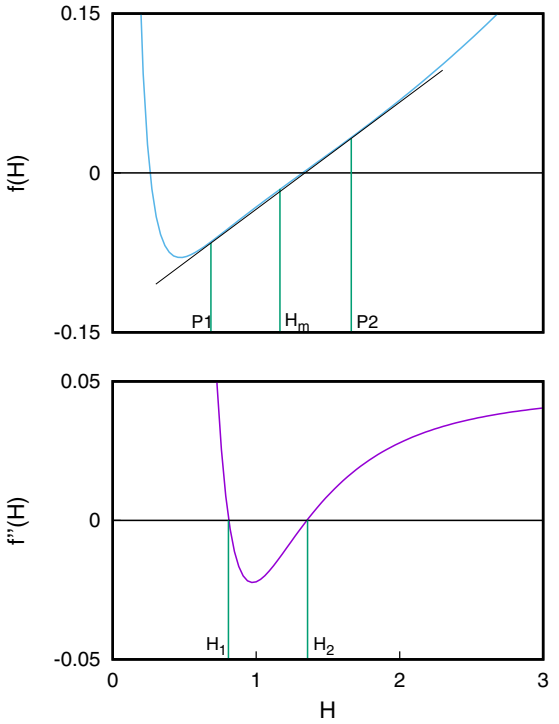

FIG. 2. Variation of dimensionless free energy $f(H)$ and its second derivative $f''(H)$ with film thickness H for a system given by Eq. (3). The parameters are $B = -0.1$, $D = 0.6$, and $G = 0.022\,87$). $P1$ and $P2$ are the thicknesses corresponding to the thinner and thicker equilibrium phases, respectively. H_m is the thickness equidistant to both $P1$ and $P2$. For $f''(H) < 0$ within the bounds of H_1 and H_2, the homogeneous thin liquid film is unstable and spontaneously segregates into the equilibrium thicknesses given by $P1$ and $P2$.

Figure 2 presents the variation of $f(H)$ (top panel) and $f''(H)$ (bottom panel) for a typical thin-liquid-film system given by Eq. (3).

The corresponding thin-film equation is now given by

$$\frac{\partial H}{\partial t} = \vec{\nabla}\cdot\{H^3\vec{\nabla}\cdot[f'(H) - \nabla^2 H]\}. \tag{4}$$

Substitution of Eq. (3) in Eq. (4) leads to the following nonlinear equation for temporal evolution of the thin-liquid-film system under gravity:

$$\frac{\partial H}{\partial t} = \vec{\nabla}\cdot\left(H^3\vec{\nabla}\cdot\left\{\frac{1}{3}\left[\frac{1-B}{(H+D)^3} + \frac{B}{H^3} + GH\right] - \nabla^2 H\right\}\right). \tag{5}$$

The linear stability analysis of Eq. (5) shows that the wavelength corresponding to the most unstable modes is

$$L_M = \frac{4\pi}{\sqrt{-f''(1)}} = 4\pi\left[\frac{1+|B|}{(1+D)^4} - |B| - \frac{G}{3}\right]^{-1/2}. \tag{6}$$

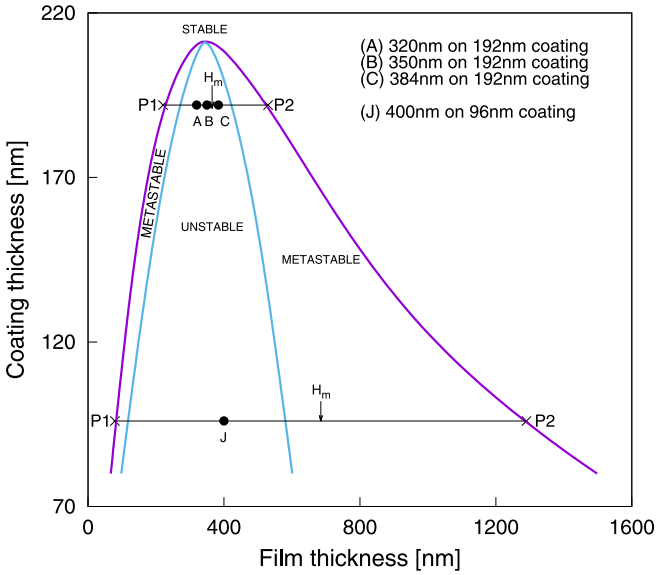

FIG. 3. Phase diagram showing the binodal and spinodal regions for a typical thin-liquid-film system under gravity.

The evolution of these instabilities leads to the formation of two true equilibrium phases as given by the Maxwell's double tangent.

The three-dimensional thin-film evolution equation is solved numerically in starting with fluctuations of small amplitude in the initial film thickness ($H \simeq 1 \pm 0.01$). The parameters D, B, and G are each varied over ranges that will render the films unstable at $H = 1$. Large-scale simulations were carried out for a system size of $(32L_M)^2$ with 32 grid points per L_M that correspond to 1024 initial sinusoidal undulations. Thus, we were able to study true MPS across several orders of length and time scales. A combination of alternating direction implicit method and Gear's algorithm has been employed along with central differencing in space with interpolation at half nodes.

III. RESULTS AND DISCUSSION

Numerical simulations show that morphological evolution during true MPS in thin-liquid-film systems depends on the initial conditions, mainly the initial film thickness h_0 and coating thickness δ. A typical phase diagram of thin-liquid-film systems under gravity given by Eq. (3) is presented in Fig. 3. Binodals (outer lines) in the phase diagram correspond to equilibrium fixed points $P1$ (thinner equilibrium phase) and $P2$ (thicker equilibrium phase) of the free-energy diagram (as shown in Fig. 2). The spinodal region (within inner spinodal lines) presents the range of unstable thicknesses. Any fluctuations in this regime amplify and cause the initial film to separate into two equilibrium thicknesses corresponding to fixed points $P1$ and $P2$. Asymmetricity in the binodals of the phase diagram (Fig. 3) reflects the asymmetricity in the free-energy functional (Fig. 2). The asymmetricity introduces two different pathways in true MPS and makes it distinct from generic spinodal phase separation (SPS). For reference, we define a parameter $H_m = (P1 + P2)/2$, which is the average value of the binodal points. In the conventional SPS of binary mixtures, the critical concentration, H_{crit}, is defined as the composition having 50%-50% of both the phases that results in bicontinuous structures. H_{crit} lies exactly halfway to the binodals and it takes only a single value, which is H_m. For thin-liquid-film systems undergoing true MPS, bicontinuous patterns corresponding to H_{crit} have been observed not only for a single value, but for any value within a narrow window of thicknesses centered around H_m. Thus, any film thickness lying in this window of H_{crit} results in a bicontinuous pattern. Depending on the relative position of initial film height H_0 with respect to H_{crit}, true MPS in unstable thin liquid films under gravity proceeds via two distinct pathways, that is, the "*direct pathway*" or the "*defect pathway*".

If the initial film thickness H_0 in the unstable region lies within the window of H_{crit} (point B in the phase diagram), the path taken by the true MPS is the direct pathway. In this pathway, both the equilibrium thicknesses $P1$ (corresponding to the thinner equilibrium phase) and $P2$ (corresponding to the thicker equilibrium phase) appear simultaneously during intermediate stages of the dynamics. If the initial film thickness H_0 lies outside the window of H_{crit} (points A or C), then the path taken by true MPS is the defect pathway. In this pathway, one of the equilibrium thicknesses appears earlier than the other equilibrium thickness during the intermediate stages of dynamics. For example, if we choose initial film thickness H_0 left to the H_{crit} (point A), then the equilibrium thickness $P1$ appears earlier than equilibrium thickness $P2$. Conversely, when H_0 lies right to the window of H_{crit} (point C), then $P2$ appears earlier than $P1$. For both these situations of defect pathway, the second equilibrium thickness appears only in the late stage of dynamics. Thus, there is a time delay between the appearance of the first and second equilibrium phases. Since one of the equilibrium thicknesses in this case appears in very late stage of the dynamics, we call it a "defect" instead of a "phase" [27]; hence, the pathway is termed as the defect pathway.

Figure 4 presents the morphological evolution of a thin liquid film undergoing true MPS through the defect pathway (point A in the phase diagram). Panels 4(a)–4(c) present the lateral view of the 3D patterns and panels 4(d)–4(f) present the corresponding top view. Random fluctuations to the surface of the thin liquid film rearrange into spinodal waves [Figs. 4(a) and 4(d)] of wavelength predicted by the linear stability analysis [Eq. (6)]. The instabilities grow until the troughs of the wave reach the thickness corresponding to the thinner equilibrium phase $P1$, resulting in domains of thin flat film and circular droplets (defects). The defects grow both radially and vertically [Figs. 4(b) and 4(e)] due to coarsening until they reach the thickness corresponding to the thicker equilibrium phase ($P2$). Once the drops reach $P2$, coarsening ceases in the vertical direction but continues laterally, resulting in flattening of the drops [Figs. 4(c) and 4(f)]. This pattern of true MPS is characterized by true equilibrium phases of "*flat film and cylindrical drops*". This sequence of morphological changes has been observed for true MPS in all unstable thin liquid films lying to the left of H_{crit} in the phase diagram. Thin films to the right of H_{crit} also undergo true MPS through the defect pathway (point C in the phase diagram), but there, $P2$ is the equilibrium phase that appears first and $P1$ is the equilibrium phase that appears after a time delay. A self-similar pattern of

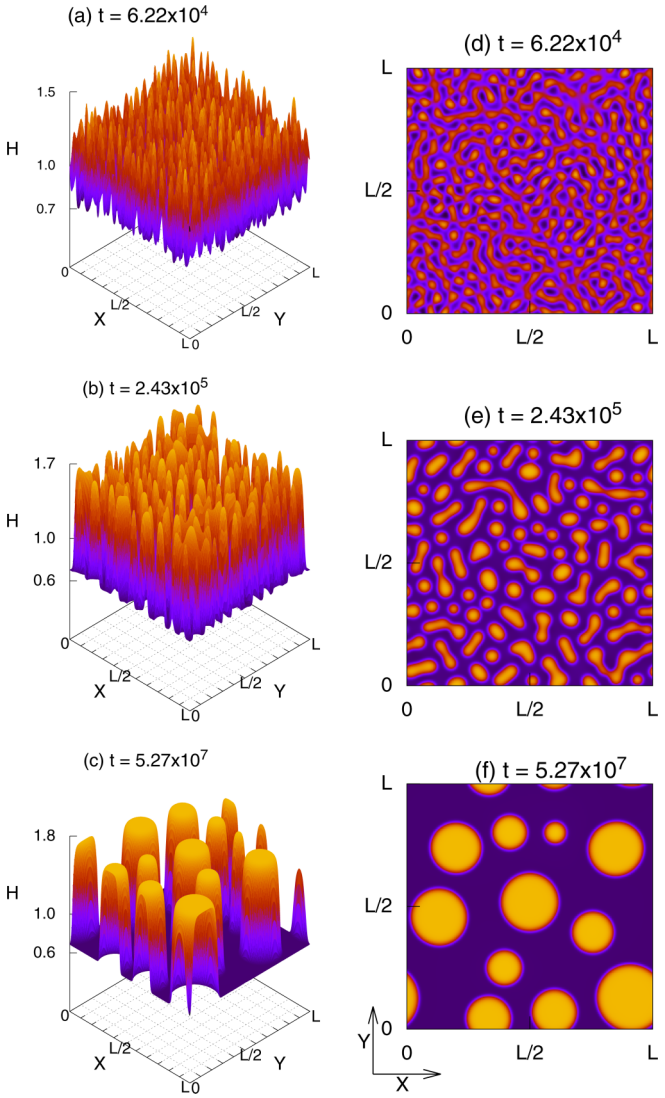

FIG. 4. Pattern formation during true MPS of a 320-nm homogeneous film on 192 nm coating, leading to a flat film and cylindrical drops (the defect pathway). The left panels present the lateral view of the system, and the corresponding right panels present the top view. Parameters are $B = -0.1$, $D = 0.6$, and $G = 0.022\,87$, and the system size is $1024L_M^2$.

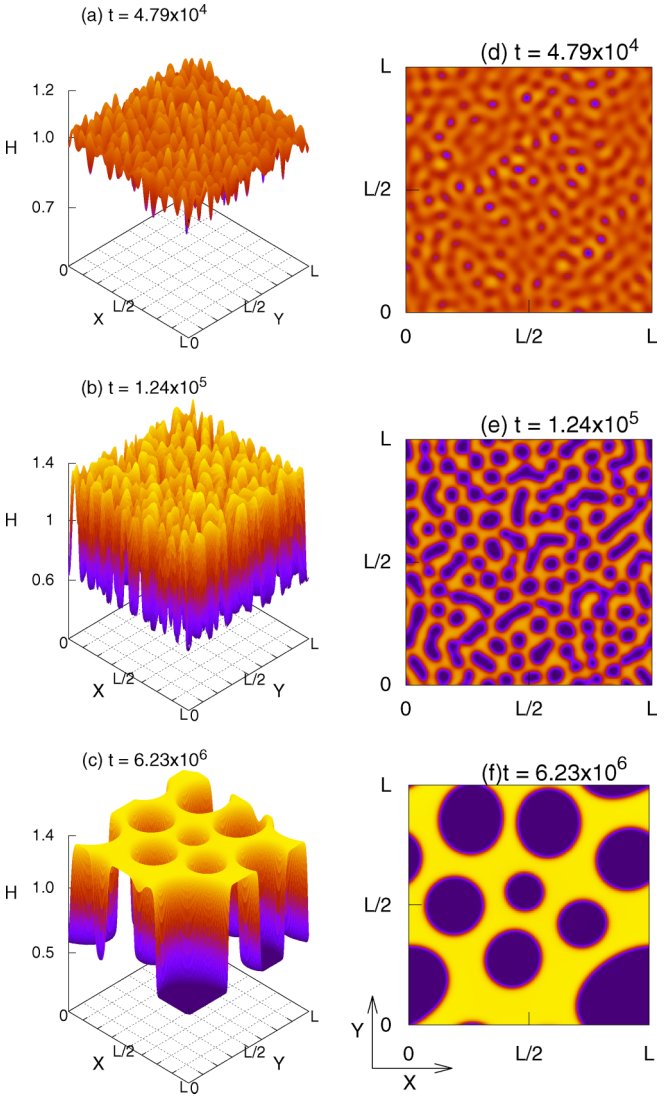

FIG. 5. Pattern formation during true MPS of a 384-nm homogeneous film on 192 nm coating, leading to circular holes and cylindrical ridges (the defect pathway). The left panels present the lateral view of the system, and the corresponding right panels present the top view. Parameters are $B = -0.1$, $D = 0.5$, and $G = 0.022\,87$, and the system size is $1024L_M^2$.

"*circular holes and cylindrical ridges*" is observed for these films, and the figures depicting the evolution are presented in Fig. 5.

Figure 6 presents the lateral [Figs. 6(a)–6(c)] and top [Figs. 6(d)–6(f)] views of a thin liquid film (point B in the phase diagram) within the region $H_{\rm crit}$ that undergoes true MPS through the "direct pathway". For these systems, both the crests and the troughs of the amplified spinodal waves [Figs. 6(a) and 6(d)] reach the thicker and thinner equilibrium phases ($P2$ and $P1$) simultaneously [Figs. 6(b) and 6(e)]. This results in a bicontinuous pattern [Figs. 6(c) and 6(f)] analogous to the critical quenching of generic spinodal phase separation in binary mixtures. *A specific kind of pattern is a signature of the initial film thickness.*

The asymmetricity of the binodals gives rise to an interesting phenomenon, wherein only some of the systems shown in the phase diagram (Fig. 3) show all three patterns. For example, for the $\delta = 192$-nm system, H_m lies inside the spinodal region; hence, depending on the initial film thickness H_0, all three patterns of true MPS can be observed (as explained above for points A, B, and C in Fig. 3). In contrast, only one pattern of *flat film and cylindrical drops* is observed for all the unstable film thicknesses (say, point J in Fig. 3) of the $\delta = 96$-nm system, wherein H_m lies outside the spinodal region. Thus, depending on whether H_m lies within the spinodal region or outside the spinodal region, we may observe either all the three patterns or only one pattern, respectively. The reason for the systems going via different pathways can be attributed to asymmetry in the free-energy functionals (i.e., finite minima having unequal depths). Normal MPS is different from the true MPS in a sense that it corresponds to a single finite minima, a single pathway, and a single pattern (flat-film phase and circular droplets).

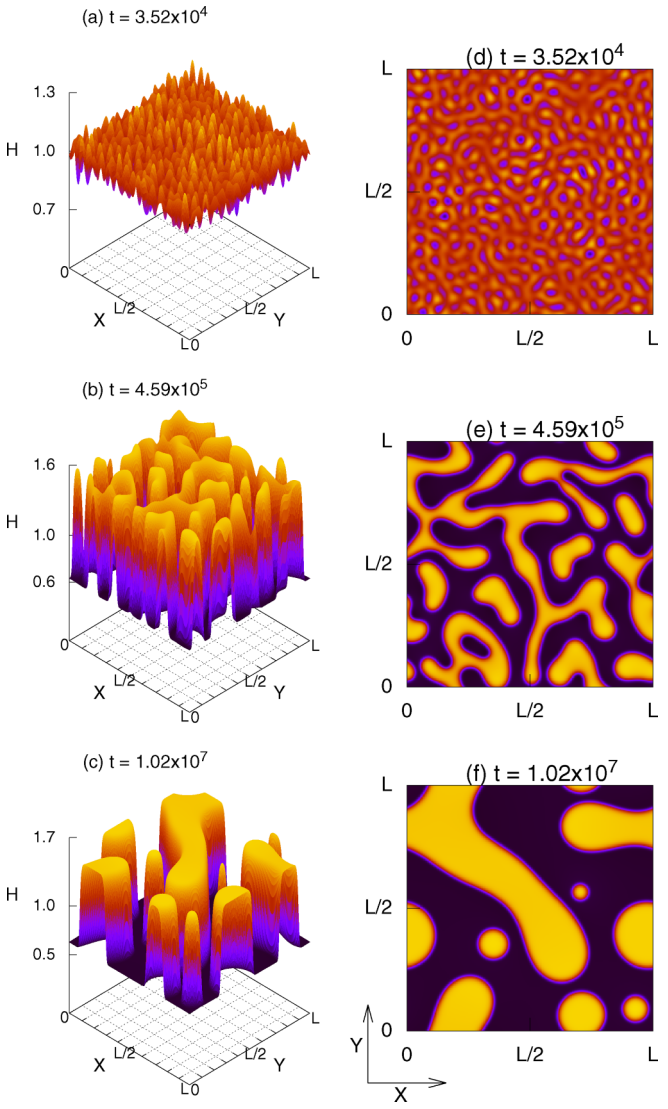

FIG. 6. Pattern formation during true MPS of a 350-nm homogeneous film on 192 nm coating, leading to a bicontinuous pattern (the direct pathway). The left panels present the lateral view of the system, and the corresponding right panels present the top view. Parameters are $B = -0.1$, $D = 0.549$, and $G = 0.022\,87$, and the system size is $1024L_M^2$.

The two pathways, i.e., the defect and the direct pathways, in true MPS are analogous to off-critical and critical quenching, respectively, in spinodal phase separation of binary mixtures. In the defect pathway, both the equilibrium phases do not appear simultaneously. As stated above, if the initial film thickness is left to $H_{\rm crit}$, equilibrium thickness corresponding to $P1$ appears earlier than $P2$. It seems as if there is a small barrier which hinders the achievement of equilibrium thickness $P2$. To understand the delay in the formation of second true phase in this pathway, we assert the fact that it is very hard to sharply define the spinodal boundary between the metastable and unstable regions [36]. In fact, the spinodal is smeared. Even though the initial film thickness is in the spinodal region, there is some effect of metastability on height fluctuations. If we move away from $H_{\rm crit}$ and choose initial film thickness H_0 more closer to the spinodal boundary, it is observed that the time delay between the appearance of two equilibrium thicknesses is longer. One of the equilibrium thicknesses near to H_0 is achieved shortly, but the growth of the second one is slowed down. This complex behavior of the defect pathway can be attributed to the asymmetricity of the free-energy functional.

Figure 7 presents the variation of height along the diagonals $H(X = Y)$ for the morphological evolutions presented in Figs. 4, 5, and 6, respectively. The delay in the formation of the second equilibrium phase during the defect pathway is clearly evident from the top and middle panels of Fig. 7, which correspond to the *flat-film phase and circular drops* and *circular holes and cylindrical ridges* patterns, respectively. Similarly, the simultaneous formation of both the phases during the direct pathway can be observed in the bottom panel of Fig. 7, which corresponds to the bicontinuous pattern.

The patterns corresponding to the defect and direct pathways of true MPS in thin-liquid-film systems have been further analyzed using statistical quantities, and the results are presented in Figs. 8 and 9. The statistical measures widely used for probing the domain structure are the equal-time correlation function,

$$C(\vec{r},t) = \langle H(\vec{R},t)H(\vec{R}+\vec{r},t)\rangle - \langle H(\vec{R},t)\rangle\langle H(\vec{R}+\vec{r},t)\rangle, \tag{7}$$

and the equal-time structure factor, which is the Fourier transform of $C(\vec{r},t)$:

$$S(\vec{k},t) = \langle \delta H(\vec{k},t)\delta H(-\vec{k},t)\rangle = \int C(\vec{r},t)\exp(i\vec{k}\cdot\vec{r})d\vec{r}. \tag{8}$$

Structure factor can be directly measured in the scattering experiments of neutrons (or x rays, light, etc.). Dynamical scaling states that at late times t, there is only one time-dependent length scale $L(t)$ in the emerging pattern. The domain morphology is independent of time when lengths are scaled by $L(t)$ [7]. In that case, $C(\vec{r},t)$ and $S(\vec{k},t)$ show the following dynamical scaling forms:

$$C(\vec{r},t) = f[\vec{r}/L(t)] = f(x), \quad x = r/L, \tag{9}$$

and

$$S(\vec{k},t) = L^d g(kL) = L^d g(y), \quad y = kL. \tag{10}$$

Here, f and g are scaling functions, x and y are the scaled variables, and d is the spatial dimensionality.

The scaling function $f(x)$, for small scaling variable x (i.e.,$r \ll L$), has a characteristic linear behavior

$$f(x) = 1 - ax + \cdots, \tag{11}$$

for both conserved and nonconserved dynamics. Here, a is a constant. This is a simple consequence of the existence of "sharp," well-defined domain walls in the systems. Because of this short-distance singularity in the correlation function, which is caused by order-parameter anticorrelations as one scans across domain boundaries, the structure factor scaling function $g(y)$ exhibits a power law tail

$$g(y) \sim y^{-(d+1)}, \quad y(= kL) \gg 1, \tag{12}$$

which is also known as the *Porod law* [37].

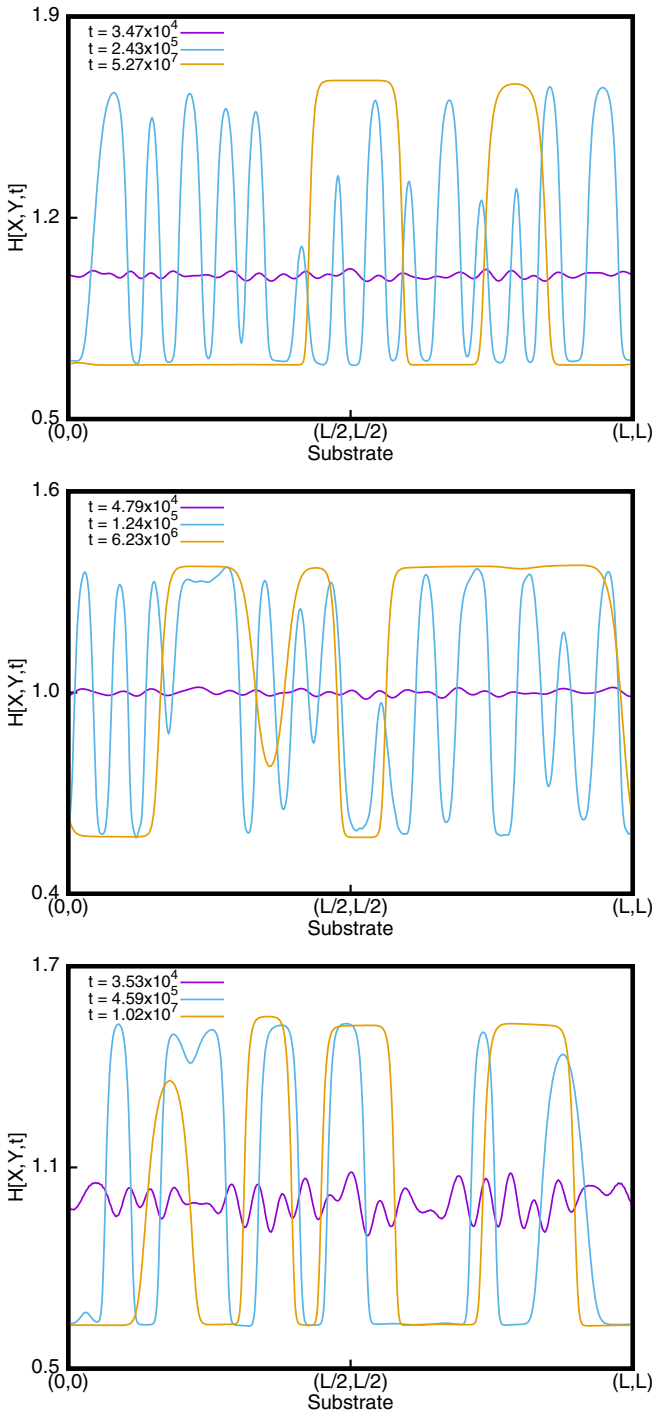

FIG. 7. Variation of the height field along a diagonal cross section ($X = Y$) for thin liquid films of thicknesses 320, 384, and 350 nm, respectively. The top, middle, and bottom panels correspond to the patterns presented in Figs. 4, 5, and 6, respectively.

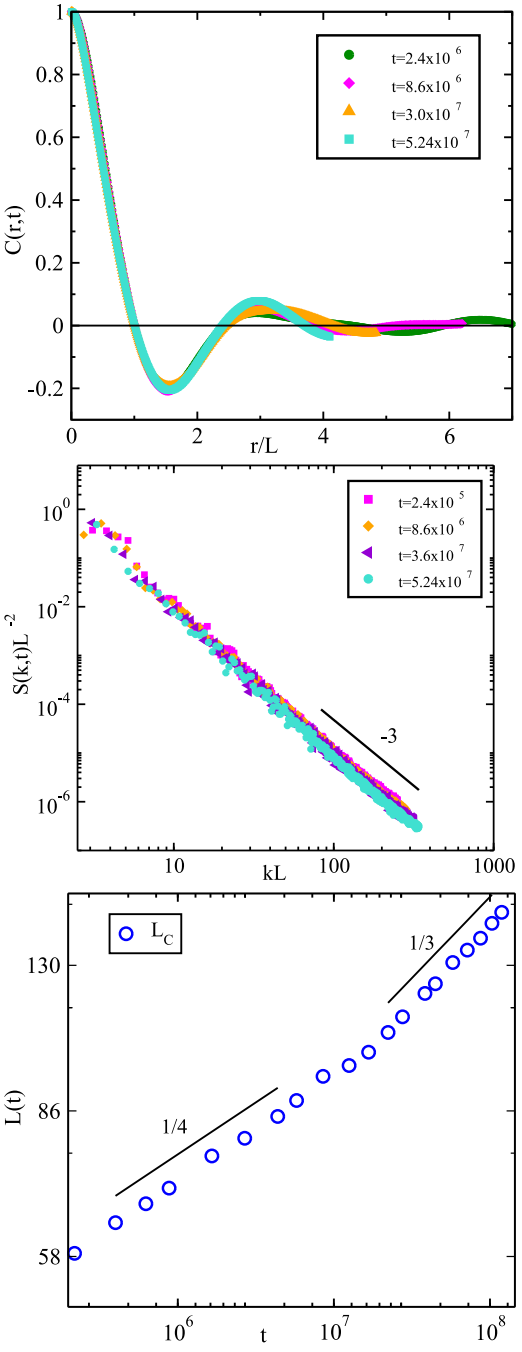

FIG. 8. Statistical measures for the evolution presented in Fig. 4. The top, middle, and bottom panels correspond to the correlation function, structure factor, and length scale of the domain size, respectively.

Our three-dimensional thin-liquid-film system (X,Y,H) is actually a $(2+1)$-dimensional system as the height fluctuation $H(X,Y)$ is a function of substrate variables X and Y. All our statistical measures are calculated in the (X,Y) plane; i.e., $d = 2$. In this plane, the morphologies are isotropic and have no directional dependence; see the right-hand frames of Figs. 4 and 6.

The top panels of Figs. 8 and 9 present the scaled correlation function at different times. These plots show that there is excellent dynamical scaling. The middle panels of Figs. 8 and 9 present the spherically averaged structure factor on a log-log scale. We observe that the structure factor tail for all the thin-liquid-film systems undergoing *true MPS* follows the *Porod law* [37], confirming the formation of sharp interfaces.

Next, we turn our attention to the characteristic length scale $L(t)$. Most physical quantities depend on time t only

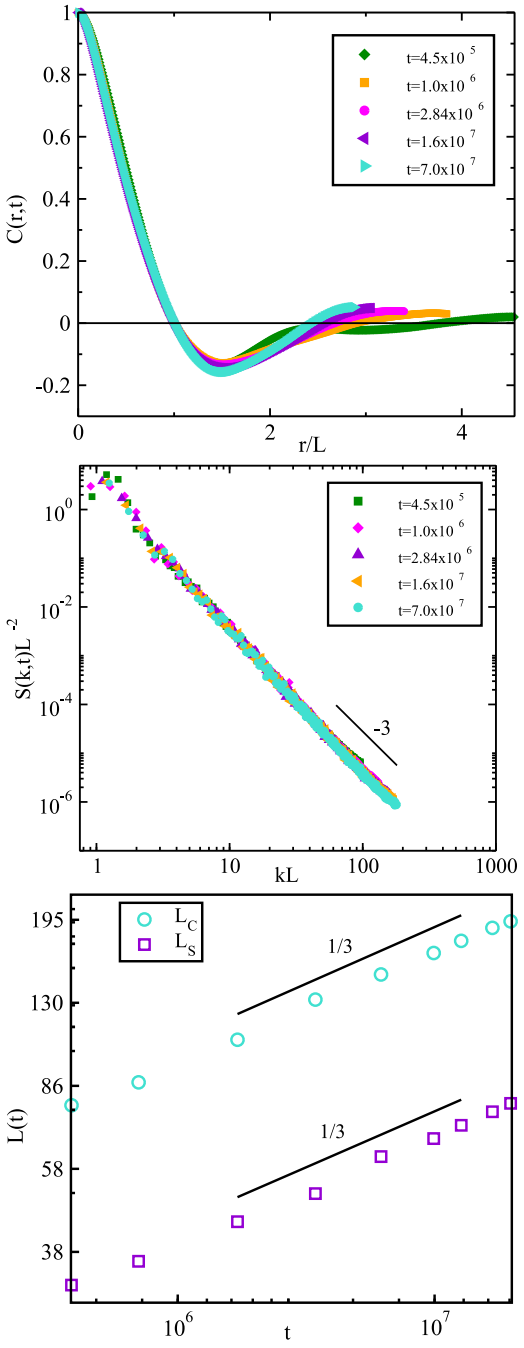

FIG. 9. Statistical measures for the evolution presented in Fig. 6. The top, middle, and bottom panels correspond to the correlation function, structure factor, and length scale of the domain size, respectively.

through this length scale. The bottom panels of Figs. 8 and 9 present the length scale calculated in two different ways, that is, from the correlation function and from the spherically averaged structure factor. (1) L_c, calculated from the correlation function, is defined as the length scale up to which $C(r,t)$ decays to half of its maximum value. (2) L_s, calculated from the spherically averaged structure factor, is defined as the inverse of the first moment of $S(k,t)$,

$$L_s = \langle k \rangle^{-1}, \tag{13}$$

where

$$\langle k \rangle = \frac{\int_0^\infty kS(k,t)dk}{\int_0^\infty S(k,t)dk}. \tag{14}$$

The asymptotic domain growth is characterized by Lifshitz-Slyozov growth law [$L(t) \sim t^{1/3}$] for both the pathways. However, in the defect pathway (Fig. 7), there is a crossover in the growth law from [$L(t) \sim t^{1/4} \rightarrow t^{1/3}$]. The exponent 1/3 is characteristic of the very late stage of spinodal phase separation in binary mixtures for the conserved order parameter. This is related to the bulk diffusion mechanism. In this kind of diffusive transport, when the length scale is $L(t)$, the growth of the domain $dL(t)/dt$ is related to diffusive flux [$\sim \gamma/L(t)^2$, where γ is the interfacial tension]:

$$\frac{dL(t)}{dt} \sim \frac{\gamma}{L(t)^2} \quad \Rightarrow \quad L(t) \sim t^{1/3}. \tag{15}$$

Similar arguments follow for exponent 1/4, where domain growth is believed to follow surface diffusion mechanism [38,39].

The crossover in growth laws has many physical implications in phase-separation dynamics. Many studies have focused on 1/4-coarsening laws, which occur due to surface diffusion [38,40,41]. In particular, the 1/4-growth law has been studied extensively in thin solid films [23–25].

To outline the stages of true MPS analogous to generic spinodal phase separation, we start from a homogeneous thin-liquid-film system, which is rendered thermodynamically unstable. This can be achieved by changing the coating thickness from the stable region in the phase diagram to the unstable or spinodal region. Such a process is generally referred to as a quench in the language of spinodal phase separation. Just after a quench, long-range correlations start developing in the system. The extent of the correlations is such that the system is rendered unstable, and, subsequently, macroscopic thickness develops inhomogeneities. In the initial stage, which is also referred to as the linear regime, the change in thickness $\delta H = [H(x,y,t) - H_0]$ is small, and the equation of motion can be linearized with respect to δH. The linear stability analysis shows that, corresponding to a particular wavelength fluctuation L_M [Eq. (6)], the height fluctuations grow most rapidly. In the second stage, the intermediate regime thickness grows, and δH becomes appreciable. The film now enters the nonlinear regime. In the third stage, we encounter the crossover regime, where we expect the thicknesses to attain the equilibrium values $P1$ and $P2$ all over the system, and sharp interfaces start appearing. Inhomogeneities in the system are very large and higher-order nonlinear terms in the gradients of H play important roles in determining the phase-order dynamics. In the fourth stage, the dynamical scaling regime, very sharp interfaces are developed, and domain growth results in larger and larger domains. The dominant mechanism in this regime is the drive to reduce curvature. The material is transported diffusively as in the Cahn-Hilliard equation of phase-separation kinetics. In the coarsening process atoms evaporate from smaller droplets and condense onto larger droplets.

IV. CONCLUSIONS

In summary, thin-liquid-film systems undergo true morphological phase separation (under gravity), whenever a Maxwell's double-tangent construction is possible. The free-energy functionals corresponding to true MPS are asymmetric, which result in the following two distinct pathways of phase separation. First is the defect pathway, whereby one of the equilibrium phases appears earlier, and the second equilibrium phase appears only after considerable coarsening of domains. A pattern on flat film and cylindrical holes is observed in thin liquid films, where the initial film thickness is closer to the thinner equilibrium phase. A pattern of circular holes and cylindrical ridges is observed in thin liquid films, where the initial film thickness is closer to the thicker equilibrium phase. Second is the direct pathway, whereby both thinner and thicker equilibrium phases appear simultaneously, resulting in a bicontinuous pattern. For systems with double-well symmetric potentials, the bicontinuous pattern for SPS is observed at a critical mixture, which is exactly halfway to the binodals. However, for the asymmetric potential systems of true MPS, the bicontinuous pattern has been observed for a range of thicknesses, centered around the thickness halfway to the binodals.

Two different scaling regimes are observed for coarsening in the defect pathway. There is a crossover from the nonequilibrium defect regime [38] to the diffusive coarsening of equilibrium domains. The corresponding growth laws are $L(t) \sim t^{1/4}$ for the coarsening of defects and $L(t) \sim t^{1/3}$ for the coarsening of equilibrium domains. The single scaling regime, corresponding to domain coarsening, $L(t) \sim t^{1/3}$, is observed for the direct pathway.

In both pathways, the system enters into the scaling regime during the late equilibrium coarsening stages and shows complete dynamical scaling. Also, the late-stage growth laws are the same as that of conventional SPS in conserved systems. The structure factor tail follows Porod's law, and the late-stage coarsening (similar to Ostwald ripening) of the dynamics follows the Lifshitz-Slyozov growth law $L(t) \sim t^{1/3}$.

Finally, the asymmetricity of the free-energy functional and the uniqueness of the "defect pathway" facilitate different perspectives on the longstanding metastable-spinodal boundary discussions. Our work shows the possibility of fabricating homogeneous nanostructures of desired thicknesses from unstable thin liquid films. This has direct implications in nanopatterning, and we hope that our results are tested in relevant experimental frameworks.

[1] J. S. Langer, *Solids Far from Equilibrium* (Cambridge University Press, Cambridge, UK, 1992).
[2] M. C. Cross and P. C. Hohenberg, Rev. Mod. Phys. **65**, 851 (1993).
[3] J. P. Gollub and J. S. Langer, Rev. Mod. Phys. **71**, S396 (1999).
[4] P. K. Maini, K. J. Painter, and H. N. P. Chau, J. Chem. Soc., Faraday Trans. **93**, 3601 (1997).
[5] A. J. Koch and H. Meinhardt, Rev. Mod. Phys. **66**, 1481 (1994).
[6] Q. Liu, A. Doelman, V. Rottschäfer, M. d. Jager, P. M. J. Herman, M. Rietkerk, and J. V. de Koppel, Proc. Natl. Acad. Sci. USA **110**, 11905 (2013).
[7] S. Puri and V. K. Wadhawan, *Kinetics of Phase Transition*, 1st ed. (CRC Press, Boca Raton, FL, 2009).
[8] R. C. Desai and R. Kapral, *Dynamics of Self-organized and self-Assembled Structures* (Cambridge University Press, Cambridge, UK, 2009).
[9] D. Gentili, G. Foschi, F. Valle, M. Cavallini, and F. Biscarini, Chem. Soc. Rev. **41**, 4430 (2012).
[10] T. Riste, *Fluctuations,Instabilities and Phase Transitions* (Plenum Press, London, 1975).
[11] J. D. Gunton and M. Droz, *Introduction to the theory of Metastable and Unstable States* (Springer Verlag, New York, 1983).
[12] A. J. Bray, Adv. Phys. **43**, 357 (1994).
[13] A. Onuki, *Phase Transition Dynamics* (Cambridge University Press, Cambridge, UK, 2002).
[14] E. Ruckenstein and R. K. Jain, J. Chem. Soc. Faraday Trans. II **70**, 132 (1974).
[15] P. de Gennes, Rev. Mod. Phys. **57**, 827 (1985).
[16] A. Oron, S. H. Davis, and S. G. Bankoff, Rev. Mod. Phys. **69**, 931 (1997).
[17] P. G. D. Gennes, F. Brochard-Wyart, and D. Quere, *Capillarity and Wetting Phenomena: Drops, Bubbles, Pearls, Waves* (Springer Verlag, New York, 2004).
[18] A. Sharma and R. Verma, Langmuir **20**, 10337 (2004).
[19] R. V. Craster and O. K. Matar, Rev. Mod. Phys. **81**, 1131 (2009).
[20] D. Bonn, J. Eggers, J. Meunier, and E. Rolley, Rev. Mod. Phys. **81**, 739 (2009).
[21] C. V. Thompson, Annu. Rev. Mater. Res. **42**, 399 (2012).
[22] R. Mukherjee and A. Sharma, Soft Matter **11**, 8717 (2015).
[23] B. K. Chakraverty, J. Phys. Chem. Solids **28**, 2401 (1967).
[24] A. Constantinescu, L. Golubović, and A. Levandovsky, Phys. Rev. E **88**, 032113 (2013).
[25] O. Pierre-Louis, Prog. Cryst. Growth Charact. Mater. **62**, 177 (2016).
[26] A. Sharma and R. Khanna, Phys. Rev. Lett. **81**, 3463 (1998).
[27] R. Khanna, N. K. Agnihotri, M. Vashishtha, A. Sharma, P. K. Jaiswal, and S. Puri, Phys. Rev. E **82**, 011601 (2010).
[28] A. Sharma and A. T. Jameel, J. Colloid Interface Sci. **161**, 190 (1993).
[29] P. K. Jaiswal, M. Vashishtha, S. Puri, and R. Khanna, Phys. Chem. Chem. Phys. **13**, 13598 (2011).
[30] I. M. Lifshitz and V. V. Slyozov, J. Phys. Chem. Solids **19**, 35 (1961).
[31] M. B. Gratton and T. P. Witelski, Phys. Rev. E **77**, 016301 (2008).
[32] C. Narayanam, A. Kumar, S. Puri, and R. Khanna, Langmuir **33**, 3341 (2017).
[33] J. W. Cahn and J. E. Hilliard, J. Chem. Phys. **28**, 258 (1958).
[34] J. W. Cahn, J. Chem. Phys. **30**, 1121 (1959).

[35] J. N. Israelachvili, *Intermolecular and Surface Forces*, 3rd ed. (Academic Press, San Diego, CA, 2011).
[36] K. Binder, in *Alloy Phase Stability*, edited by G. M. Stocks and A. Gonis (Kluwer Academic Press, Dordrecht, 1989).
[37] G. Porod, in *Small-angle X-ray Scattering*, edited by O. Glatter and O. Kartky (Academic Press, San Diego, CA, 1982).
[38] Y. Oono and S. Puri, Phys. Rev. Lett. **58**, 836 (1987).
[39] K. Kawasaki and T. Ohta, Prog. Theor. Phys. **68**, 129 (1982).
[40] F. Otto and E. Weinan, J. Chem. Phys. **107**, 10177 (1997).
[41] C. Sagui and M. Grant, Phys. Rev. E **59**, 4175 (1999).